Chapter 1

Introduction

Modern demands on airport security require fast baggage screening devices that examine non-intrusively pieces of luggage for the presence of explosives and illicit substances. The ultimate choice of the system that is adopted is often determined by local standards for throughput, detection sensitivity and false-alarm rate.

For first level baggage inspection most airports use conventional transmission x-ray scanners or more sophisticated Computed Tomography (CT) systems. Both technologies are fully automated and are highly rated for performance and throughput. The degree to which x-rays penetrate objects depends on the atomic number and density of the materials inside. This property is exploited to localize dense materials embedded in less dense materials.

A major drawback of these systems is the physical limit to material discrimination given by the differences of the attenuation properties inside the bags. As a consequence x-ray transmission technologies produce a significant number of false alarms, i.e. alarms from harmless materials having similar total attenuation coefficients to the threat substance. At airports with high passenger traffic volumes, even modest false alarm rates lead to an enormous number of bags requiring additional visual and manual inspection by operators. This procedure increases

Figure 1.1: *The baggage screening system GE XRD* 3500^{TM} *is fully automated and TSA certified. Image courtesy GE Security Germany GmbH.*

operating costs and processing time for passenger baggage, which in turn brings inconvenience for passengers.

X-ray diffraction (XRD) has been identified as a complementary technology to conventional X-ray transmission because of its capability to reduce the false alarm rate when combined with CT [1, 2]. The only commercial XRD-based explosive detection system, which is available on the market today and certified by the American Transport Security Agency (TSA) so far, is the GE XRD 3500^{TM} (see Fig. 1.1). The system is already installed at several European airports and is typically used as the second level of automatic inspection. The location of the threat as detected by the first level CT system is transferred to the second where a localized XRD scan is performed. The measurement yields material specific information about the molecular structure of individual volume elements within inhomogeneous, extended objects. Diffraction profiles can be used as a fingerprint of the material for comparison with library functions. The XRD fingerprint can help to resolve alarms from the first level detection system without opening the baggage and avoiding operator intervention.

The GE XRD 3500^{TM} technology is based on the energy-dispersive method of x-ray diffraction, also known as white-beam diffraction. The sample is irradiated by a polychromatic beam and the x-rays scattered in a small angle from the forward direction are analyzed using a stationary energy-resolving detector. The method has been extended to provide an image forming technique called Energy-dispersive X-ray Diffraction Tomography (EDXDT) [3, 4]. A test system with pencil-beam geometry has been constructed to demonstrate that EDXDT permits the measurement of an x-ray diffraction pattern from a small volume element (voxel) within an extended object. Tomographic information is obtained by directly localising the scatter voxel using mechanical collimation. Potential applications have been discussed in the fields of medical diagnosis, foodstuff contamination detection and explosives detection [4, 5, 6]. The developement of a highly application-specific system design, employing a cone-beam geometry for parallel data acquisition from different voxels, provided the basis for the prototype of an airport baggage screening system [7, 8, 9].

A related imaging technique is Coherent Scatter Computed Tomography (CSCT), which combines the methods of XRD and CT reconstruction [10, 11, 12]. The spatial distribution of diffraction profiles in a slice of an extended object is reconstructed from scatter projections measured in various directions. Pioneering work in this field started with a pencil-beam geometry employing angle-dispersive collection of diffraction data [10, 11, 13, 14, 15]. With the advent of multislice CT systems it became possible to illuminate a whole object slice using a fan-shaped primary beam [12, 16, 17, 18]. Major improvements in momentum transfer resolution of diffraction data could be achieved by using energy-resolving detectors which can be operated at room temperature and fabricated in compact arrays [19, 20, 21]. Reconstruction time could be reduced by introducing fast computer algorithms based on the filtered back-projection technique [22, 23].

Energy-dispersive X-ray Diffraction Tomography (EDXDT) and Coherent Scatter Computed Tomography (CSCT) can be regarded as two techniques for X-ray

Diffraction Imaging (XDI). These new radiographic methods are currently being used more extensively for the detection and identification of explosives and drugs [24]. Technological innovations in the fields of multi focus x-ray sources as well as pixellated energy-resolving semiconductor detectors made it possible to introduce alternative geometries for direct tomographic, energy-dispersive XDI systems, including direct and inverse fan-beam geometries [25].

As a consequence of the London transatlantic plot in 2006, in which concentrated hydrogen peroxide was to have been mixed with a fuel such as acetone to create an explosive mixture during the flight, passengers have been required to remove liquids from their hand luggage prior to boarding. There is a prevailing operational need in the civil aviation industry for a screening technology capable of detecting and distinguishing liquid explosives and their constituents from benign liquids, including pure liquids, solutions and gels.

The aim of the present work is to investigate Inverse Fan-beam XDI and its capability of identifying liquid and amorphous substances. The thesis is structured as follows:

- **Chapter 2** provides the fundamental physics of x-ray interactions with matter with special emphasis on liquids and amorphous solids.

- **Chapter 3** presents design studies connected to the Inverse Fan-beam XDI system. The geometrical configuration of the major x-ray components is discussed and evaluated using numerical procedures.

- **Chapter 4** describes the synchrotron facilities, instrumentation and experimental methods used for aquisition of x-ray diffraction data. The measured diffraction profiles from liquid and amorphous substances which are of special importance for security applications are presented.

- Studies on liquids identification with applications in explosives detection are presented in **Chapter 5**. The theoretical considerations are evaluated using free atom scattering functions as well as measured diffraction profiles.

- A summary of the results and an outlook on future developments is given in **Chapter 6**.

Chapter 2

Theoretical background

2.1 X-ray cross-sections

X-rays interact with matter via a number of processes that have been extensively investigated. The probability of a particular process varies with the atomic number of the target and photon energy of the x-ray beam and is generally described by an interaction cross-section, σ. In the 20-500 keV energy region used for diagnostic and industrial radiology, the principle mechanisms are coherent scattering, incoherent scattering, and photoelectric absorption. The individual particle cross-sections contribute linearly to the total interaction cross-section,

$$\sigma = \sigma_{coh} + \sigma_{inc} + \sigma_{abs}. \tag{2.1}$$

Figures 2.1 and 2.2 show total and partial cross-sections for a light element (carbon, Z=6), a transition metal (copper, Z=29) and a heavy element (lead, Z=82). The calculations have been carried out using the NIST web program called XCOM which generates cross-sections and attenuation coefficients for elements, compounds and mixtures at energies between 1 keV and 100 GeV [26]. Cross-sections are commonly expressed in units of *barns per atom*. *One barn* is 10^{-28} m^2, which

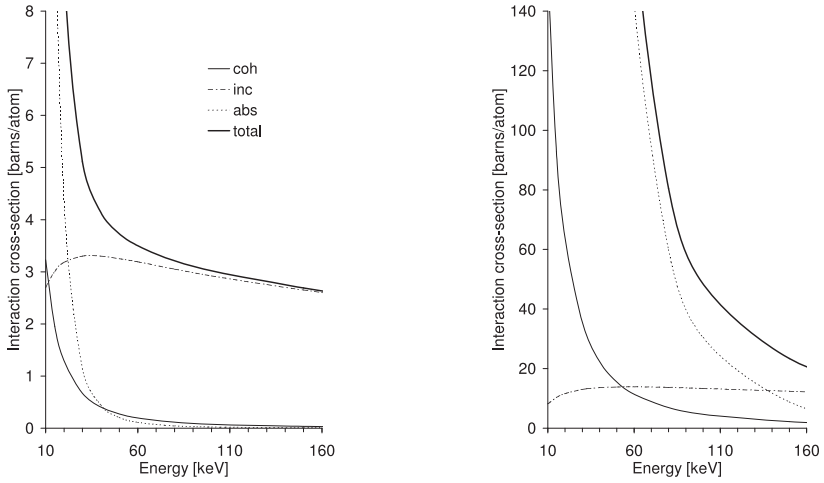

(a) Carbon (Z=6) (b) Copper (Z=29)

Figure 2.1: *Total photon interaction cross-section (bold line) and partial interaction cross-sections for coherent scattering (solid line), incoherent scattering (dash-dotted line), and photoelectric absorption (dotted line).*

is approximately the cross sectional area of a uranium nucleus. The total interaction cross-section is closely related to the linear attenuation coefficient, μ, by the number density, n, of the atoms in the target.

$$\mu = n\ \sigma \tag{2.2}$$

The number density can be evaluated by

$$n = \frac{N_A \cdot \rho}{M}, \tag{2.3}$$

where M [kg/mol] is the molar mass, ρ [kg/m^3] is the mass density and N_A [1/mol] is the Avogadro constant. When an x-ray beam passes through matter each interaction process contributes to a reduction in the beam intensity, I. The gradient along the infinitesimal distance, dz, at a depth, z, from the surface is described by the linear attenuation coefficient.

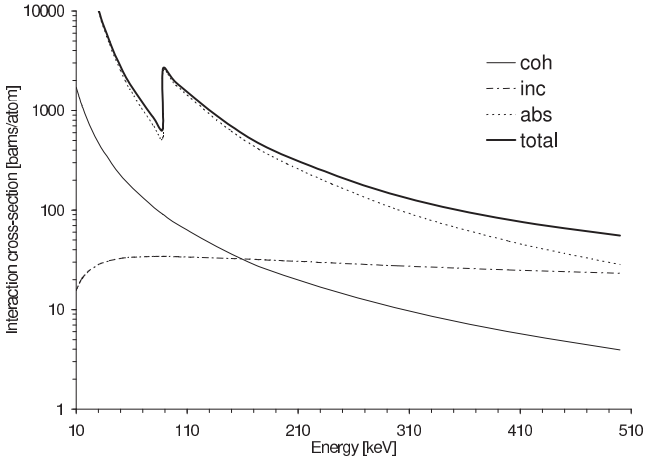

Figure 2.2: *Lead (Z=82). Total photon interaction cross-section (bold line) and partial interaction cross-sections for coherent scattering (solid line), incoherent scattering (dash-dotted line), and photoelectric absorption (dotted line).*

$$-\frac{dI}{dz} = \mu(z)\ I(z) \tag{2.4}$$

For an incident beam intensity I_0 at the surface

$$I(z) = I_0\ \exp\left(-\int_0^z \mu(z')\ dz'\right). \tag{2.5}$$

The cross-section is an important quantity since it provides the basis for quantitative analysis of the interaction processes.

2.2 Photoelectric absorption

The excitation of electrons bound in atoms by photons is called photoelectric absorption. The electron is ejected with a kinetic energy equal to the incident photon energy minus its binding energy and minus the work function. The work

function is the minimum energy that must be given to an electron to liberate it from the surface of a particular substance. The largest contribution to the photoelectric absorption is made by electrons in the inner shells where the binding energy can be similar to the incident x-ray energy (atomic photoelectric effect resonances). For absorption in the K-shell and energies used in diagnostic radiology the cross-section is approximately given by

$$\sigma_{abs} = \frac{8\pi}{3}\, r_e^2\, \frac{4\sqrt{2}}{137^4}\, Z^5\, K^{-\frac{7}{2}}. \tag{2.6}$$

Z is the atomic number and K the photon energy in units of the electron rest mass energy [27]. The photoelectron interaction probability increases continuously with increasing atomic number and decreasing photon energy. The interaction cross-section drops abruptly for photon energies below the binding energy of an electronic shell. The discontinuity is clearly visible at the K-shell of lead in Fig. 2.2. If the photon energy is less than the K-shell transition energy, only the outer shells contribute to the interaction cross-section.

2.3 Coherent scattering

Coherent scattering from free electrons

When an electromagnetic wave interacts with a charged particle, the electric and magnetic components of the wave exert a Lorentz force on the particle, setting it in motion. Since the wave is periodic in time, so is the motion of the particle. The particle is accelerated and, consequently, emits radiation. More exactly, energy is absorbed from the incident wave by the particle and re-emitted as electromagnetic radiation. The frequency of the re-emitted electromagnetic radiation will be that of the induced oscillations. Such a process is clearly equivalent to the scattering of the electromagnetic wave by the particle and is fully described in classical electrodynamics by the Thomson formula,